

Structural Mutations That Probe the Interactions between the Catalytic and Dianion Activation Sites of Triosephosphate Isomerase

Xiang Zhai,[†] Tina L. Amyes,[†] Rik K. Wierenga,[‡] J. Patrick Loria,[§] and John P. Richard^{*,†}

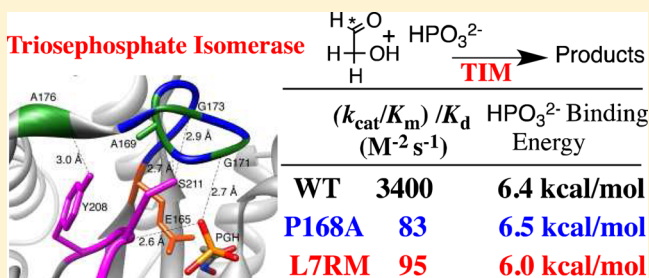
[†]Department of Chemistry, University at Buffalo, Buffalo, New York 14260, United States

[‡]Department of Biochemistry and Biocenter Oulu, University of Oulu, P.O. Box 3000, FIN-90014 Oulu, Finland

[§]Department of Chemistry and Department of Molecular Biophysics and Biochemistry, Yale University, New Haven, Connecticut 06520, United States

S Supporting Information

ABSTRACT: Triosephosphate isomerase (TIM) catalyzes the isomerization of dihydroxyacetone phosphate to form D-glyceraldehyde 3-phosphate. The effects of two structural mutations in TIM on the kinetic parameters for catalysis of the reaction of the truncated substrate glycolaldehyde (GA) and the activation of this reaction by phosphite dianion are reported. The P168A mutation results in similar 50- and 80-fold decreases in $(k_{\text{cat}}/K_{\text{m}})_{\text{E}}$ and $(k_{\text{cat}}/K_{\text{m}})_{\text{E:HP}}$, respectively, for deprotonation of GA catalyzed by free TIM and by the TIM-HPO₃²⁻ complex. The mutation has little effect on the observed and intrinsic phosphite dianion binding energy or the magnitude of phosphite dianion activation of TIM for catalysis of deprotonation of GA. A loop 7 replacement mutant (L7RM) of TIM from chicken muscle was prepared by substitution of the archaeal sequence 208-TGAG with 208-YGGS. L7RM exhibits a 25-fold decrease in $(k_{\text{cat}}/K_{\text{m}})_{\text{E}}$ and a larger 170-fold decrease in $(k_{\text{cat}}/K_{\text{m}})_{\text{E:HP}}$ for reactions of GA. The mutation has little effect on the observed and intrinsic phosphodianion binding energy and only a modest effect on phosphite dianion activation of TIM. The observation that both the P168A and loop 7 replacement mutations affect mainly the kinetic parameters for TIM-catalyzed deprotonation but result in much smaller changes in the parameters for enzyme activation by phosphite dianion provides support for the conclusion that catalysis of proton transfer and dianion activation of TIM take place at separate, weakly interacting, sites in the protein catalyst.



Triosephosphate isomerase (TIM) catalyzes the stereospecific and reversible conversion of dihydroxyacetone phosphate (DHAP) to (R)-glyceraldehyde 3-phosphate (GAP),^{1,2} by a proton transfer mechanism through enzyme-bound *cis*-enediolate reaction intermediates (Scheme 1). The carboxylate anion side chain of Glu165/167^a functions as a Brønsted base to abstract a proton from the α -carbonyl carbon of the bound substrate,^{3–6} and the developing negative charge at the carbonyl carbon is stabilized by hydrogen bonding to the neutral imidazole side chain of His95.^{7–9} The isomerization reaction is completed by reprotonation of the enediolate intermediate at the adjacent carbon (Scheme 1).

The results of more than 50 years of studies of TIM have served to define what is known about the mechanism for enzymatic catalysis of deprotonation of carbon, and the important problems that remain to be resolved.^{1,10–14} It was suggested that catalysis by TIM is “not different, just better” than catalysis by small molecules.¹⁵ TIM is “better” than small molecules in the sense that the catalytic side chains of TIM are activated for catalysis at the enzyme active site.^{16–21} The 11-residue (166–176)^a flexible phosphodianion gripper loop 6 of TIM from chicken muscle (*c*TIM) plays an important role in enzyme activation.^{22–26} Loop 6 is open at unliganded TIM,

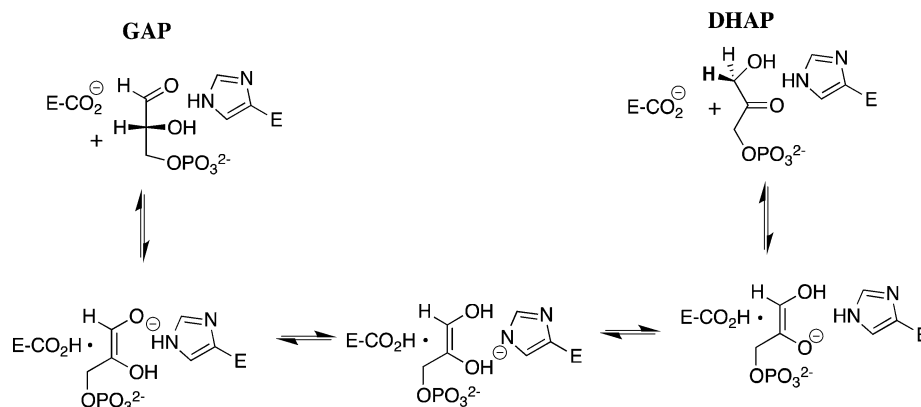
allowing the substrate access to the enzyme active site. The binding of substrate to TIM is followed by loop closure that sequesters the ligand from interaction with solvent water and strips several solvent molecules from the enzyme active site.²⁷ The closure of loop 6 is accompanied by a conformational change of loop 7, and this loop closure is driven energetically by formation of hydrogen bonds between the backbone amides of Gly171 of loop 6 and Ser211 of loop 7 to the ligand phosphodianion, along with the formation of interloop hydrogen bonds between loop 6 and the 208-YGGS motif of loop 7.^{27–29}

Two experiments provide reinforcing pieces of evidence that interactions between loop 6 of TIM and the substrate phosphodianion activate TIM for catalysis of isomerization. (1) Truncation of residues Ile170–Gly173 at the tip of loop 6 of *c*TIM and the introduction of a peptide bond between Ala169 and Lys174 disrupt loop–phosphodianion interactions but should not affect the protein fold.²² The 10⁵-fold decrease in k_{cat} and the much smaller 2.3-fold increase in K_{m} determined for isomerization of GAP catalyzed by this loop deletion mutant

Received: July 28, 2013

Published: August 2, 2013

Scheme 1



of *c*TIM show that the full loop 6 is required to observe robust turnover of the bound substrate. (2) Truncation of the phosphodianion from GAP leads to a 10⁹-fold reduction in $k_{\text{cat}}/K_{\text{m}}$ for TIM-catalyzed isomerization of the minimal neutral substrate glycolaldehyde (GA).³⁰ The binding of phosphite dianion to TIM results in an ~1000-fold increase in the catalytic activity of TIM toward deprotonation of GA.³⁰ A comparison of the TIM-catalyzed reactions of the whole substrate GAP and the substrate pieces shows that 50% of the total 11 kcal/mol intrinsic binding energy of the phosphodianion of GAP may be recovered as phosphite dianion activation of the reaction of GA.³⁰

The determination of the mechanism for phosphite dianion activation of TIM is a difficult and significant problem, whose solution is broadly relevant to the mechanism of phosphite dianion activation of several enzymatic reactions, including enzyme-catalyzed decarboxylation,³¹ proton transfer,^{32,33} hydride transfer,³⁴ phosphoryl transfer,³⁵ and reductoisomerization reactions,³⁶ and to the more general problem of the mechanism for the utilization of the intrinsic substrate binding energy in stabilizing the transition states for enzymatic reactions.^{37,38} We report here the results of a study of the effect of two structural mutations of TIM on enzyme activation by phosphite dianion.

The 208-YGGG sequence at residues 208–211 is generally observed for loop 7 of TIM.²⁹ The 208-TGAG sequence commonly found at archaeal organisms has been substituted for 208-YGGG of *c*TIM, and the resulting loop 7 replacement mutant (L7RM) of *c*TIM exhibits a 200-fold decrease in $k_{\text{cat}}/K_{\text{m}}$ for isomerization of GAP and DHAP.²⁸ TROSY-Hahn Echo³⁹ and TROSY-selected R_{1ρ}⁴⁰ experiments indicate that this mutation of loop 7 results in a doubling of the rate of conformational exchange associated with active site loop motion and a reduction in the coordinated motion of loop 6 relative to that of wild-type TIM.²⁸ These results provide evidence that interactions between loops 6 and 7 are necessary to ensure the proper chemical environment for the enzymatic reaction and that interloop interactions play a significant role in modulating the chemical dynamics near the active site.²⁸ The P168A mutant of TIM from *Trypanosoma brucei brucei* (*Tbb*TIM) was targeted for study, because of the expectation that the excellent high-resolution X-ray crystal structures for the free and liganded P168A mutant enzyme would provide a structure-based rationalization for the effect of the mutation on the kinetic parameters for enzyme activation by phosphite dianion.⁴¹

We report here that the 208-TGAG for 208-YGGG loop 7 replacement mutation of *c*TIM and the P168A mutation of *Tbb*TIM result in decreases in the kinetic parameters for enzyme-catalyzed deprotonation of [1-¹³C]GA in the absence and presence of HPO₃²⁻ that are similar to the ~100-fold decreases in k_{cat} for the reaction of the whole substrate GAP. Both the P168A and loop 7 replacement mutant enzyme-catalyzed reactions of [1-¹³C]GA are strongly activated by phosphite dianion, and the activation is similar to that for the corresponding wild-type enzyme. The observation that these structural mutations cause a significant decrease in the reactivity of TIM toward catalysis of deprotonation of [1-¹³C]GA but have little effect on enzyme activation by phosphite dianion shows that it is possible to modify the catalytic activity at the site that conducts carbon deprotonation without severely affecting enzyme activation at the dianion binding site.

EXPERIMENTAL PROCEDURES

Materials. Rabbit muscle α -glycerol-3-phosphate dehydrogenase and glyceraldehyde-3-phosphate dehydrogenase were purchased from Sigma. These enzymes were exhaustively dialyzed against 20 mM triethanolamine buffer (pH 7.5) at 7 °C prior to being used in coupled enzyme assays. Bovine serum albumin was purchased from Roche. DEAE Sepharose Fast Flow was purchased from GE Healthcare. D,L-Glyceraldehyde-3-phosphate diethyl acetal (barium salt), dihydroxyacetone phosphate (lithium salt), NADH (disodium salt), Dowex 50WX4-200R, triethanolamine hydrochloride, and imidazole were purchased from Sigma. Hydrogen arsenate heptahydrate and sodium phosphite (dibasic, pentahydrate) were purchased from Fluka and were dried under vacuum prior to use.³⁰ [1-¹³C]Glycolaldehyde (99% enrichment of ¹³C at C-1, 0.09 M in water) was purchased from Omicron Biochemicals. Deuterium oxide (99% D) and deuterium chloride [35% (w/w), 99.9% D] were purchased from Cambridge Isotope Laboratories. Sodium 2-phosphoglycolate was synthesized by following a published procedure.⁴² Imidazole was recrystallized from benzene. All other chemicals were reagent grade or better and were used without further purification.

Preparation of Enzymes. Expression vectors (pET-15b) containing genes encoding wild-type and L7RM *c*TIM were available from a previous study.²⁸ These plasmids were introduced into the TIM-deficient *tpiA*⁻ λ DE3 lysogenic strain of *Escherichia coli*, FB215471(DE3), which was a generous gift from B. Miller.⁴³ Cells were grown overnight at 37 °C in 200–300 mL of Luria broth that contained 100 μ g/mL ampicillin

and 40 $\mu\text{g}/\text{mL}$ kanamycin. These cultures were diluted into 6 L of the same medium and incubated at 37 °C until an OD_{600} of 0.6 was reached. Protein expression was then induced by the addition of 0.6 mM isopropyl 1-thio-D-galactoside (IPTG) followed by incubation for an additional 6 h. The cells were harvested, suspended in 25 mM Tris-HCl (pH 8.0, 25 mL), and stored at -80 °C. Wild-type and L7RM ϵ TIMs were purified according to a published procedure.⁴⁴ Fractions from the final DEAE-Sepharose ion exchange column that were judged to be homogeneous by gel electrophoresis were pooled, concentrated, and stored in 25 mM Tris-HCl (pH 8.0) at an ionic strength of 0.1 (NaCl) containing 20% glycerol at -80 °C. The protein concentration was determined from the absorbance at 280 nm using extinction coefficients of 33500 $\text{M}^{-1} \text{cm}^{-1}$ for wild-type ϵ TIM and 32000 $\text{M}^{-1} \text{cm}^{-1}$ for L7RM ϵ TIM that were calculated using the ProtParam tool available on the ExPASy server.^{45,46}

The pET3a plasmid containing the gene encoding P168A mutant *Tbb*TIM was prepared in an earlier study.⁴¹ P168A mutant *Tbb*TIM was overexpressed in *E. coli* BL21 pLys S grown in LB medium at 18 °C and purified by chromatography over a CM Sepharose column, as described previously.⁴⁷ Fractions that were judged to be homogeneous by gel electrophoresis were pooled, concentrated, and stored at -80 °C in 25 mM TEA (pH 8.0) that contains 20% glycerol at an ionic strength of 0.15 (NaCl). The protein concentration was determined from the absorbance at 280 nm using an extinction coefficient of 35000 $\text{M}^{-1} \text{cm}^{-1}$ calculated using the ProtParam tool available on the ExPASy server.^{45,46}

General Methods. The solution pH or pD was determined at 25 °C using an Orion model 720A pH meter equipped with a radiometer pHC4006-9 combination electrode that was standardized at pH 7.0 and 10.0. Values of pD were calculated by adding 0.40 to the observed reading of the pH meter.⁴⁸ Stock solutions of D,L-glyceraldehyde 3-phosphate (D,L-GAP) were prepared by hydrolysis of the corresponding diethyl acetal (barium salt) using Dowex 50WX4-200R (H^+ form) in boiling H_2O , as described previously.¹⁴ The resulting solutions were stored at -20 °C and were adjusted to pH 7.5 by the addition of 1 M NaOH prior to use in enzyme assays. Stock solutions of buffers,^{30,49} phosphite, [$1\text{-}^{13}\text{C}$]glycolaldehyde ([$1\text{-}^{13}\text{C}$]GA),⁴⁹ and 2-phosphoglycolate (PGA)¹⁶ were prepared as described in previous work.

Enzyme Assays. All enzyme assays were conducted at pH 7.5, 25 °C, and an ionic strength of 0.1 (NaCl) according to procedures described in our previous work. α -Glycerol-3-phosphate dehydrogenase was assayed by monitoring the oxidation of NADH by DHAP,¹⁴ and glyceraldehyde-3-phosphate dehydrogenase was assayed by monitoring the enzyme-catalyzed reduction of NAD^+ by GAP.²⁰ The TIM-catalyzed isomerization of GAP was monitored by coupling the formation of the product DHAP to the oxidation of NADH catalyzed by α -glycerol-3-phosphate dehydrogenase.^{14,49} The TIM-catalyzed isomerization of DHAP was monitored by coupling the formation of the product GAP to the reduction of NAD^+ catalyzed by glyceraldehyde-3-phosphate dehydrogenase in the presence of 2–10 mM arsenate.^{20,50}

Values of k_{cat} and K_{m} for TIM-catalyzed isomerization of GAP were determined from the nonlinear least-squares fit of the initial velocity data to the Michaelis–Menten equation. Values of K_{i} for competitive inhibition of TIM by PGA at pH 7.5 [ionic strength of 0.1 (NaCl)] were determined by examining the effect of increasing concentrations of GAP on

the initial velocity of TIM-catalyzed isomerization in the presence of two fixed concentrations of PGA. In these assays, the amount of α -glycerol-3-phosphate dehydrogenase coupling enzyme was increased to overcome its inhibition by PGA. Values of k_{cat} and K_{m} for TIM-catalyzed isomerization of DHAP and the values of K_{i} for competitive inhibition by arsenate were determined by examining the effect of increasing concentrations of DHAP on the initial velocity of TIM-catalyzed isomerization in the presence of 2, 5, and 10 mM arsenate.

^1H NMR Analyses. ^1H NMR spectra at 500 MHz were recorded in D_2O at 25 °C using a Varian Unity Inova 500 spectrometer that was shimmed to give a line width of ≤ 0.5 Hz for the most downfield peak of the double triplet due to the C-1 proton of the hydrate of [$1\text{-}^{13}\text{C}$]GA.⁴⁹ Spectra (16–64 transients) were obtained using a sweep width of 6000 Hz, a pulse angle of 90°, and an acquisition time of 6 s. A total relaxation delay of 120 s ($>8T_1$) between transients was used to ensure that accurate integrals were obtained for the protons of interest.^{51,52} Baselines were subjected to a first-order drift correction before determination of integrated peak areas. Chemical shifts are reported relative to that for HOD at 4.67 ppm.

TIM-Catalyzed Reactions of [$1\text{-}^{13}\text{C}$]GA in D_2O Monitored by ^1H NMR. The unactivated and phosphite dianion-activated reactions of [$1\text{-}^{13}\text{C}$]GA catalyzed by wild-type ϵ TIM, L7RM ϵ TIM, and P168A mutant *Tbb*TIM in D_2O at 25 °C were monitored by ^1H NMR spectroscopy, as described previously.⁴⁹ The enzymes were exhaustively dialyzed against 30 mM imidazole buffer (20% free base) in D_2O at pD 7.0 [ionic strength of 0.1 (NaCl)] for reactions in the absence of phosphite dianion, or against 30 mM imidazole buffer (20% free base) in D_2O at pD 7.0 (ionic strength of 0.024) for reactions in the presence of phosphite dianion. The unactivated TIM-catalyzed reactions of [$1\text{-}^{13}\text{C}$]GA in the absence of phosphite dianion were initiated by the addition of enzyme to give reaction mixtures (850 μL) containing 20 mM [$1\text{-}^{13}\text{C}$]GA, 20 mM imidazole (20% free base) in D_2O at pD 7.0 and an ionic strength of 0.1, and 0.34 mM wild-type ϵ TIM, 0.48 mM L7RM ϵ TIM, or 0.22–0.49 mM P168A *Tbb*TIM. The TIM-catalyzed reactions of [$1\text{-}^{13}\text{C}$]GA in the presence of phosphite dianion were initiated by the addition of enzyme to give reaction mixtures (850 μL) containing 20 mM [$1\text{-}^{13}\text{C}$]GA, 20 mM imidazole (20% free base), up to 20 mM HPO_3^{2-} (1:1 dianion:monoanion) in D_2O at pD 7.0 and an ionic strength of 0.1 (NaCl), and 9–30 μM wild-type ϵ TIM, 90–520 μM L7RM ϵ TIM, or 60–350 μM P168A *Tbb*TIM. In each case, 750 μL of the reaction mixture was transferred to an NMR tube, the ^1H NMR spectrum was recorded immediately, and spectra were then recorded at regular intervals. The remaining reaction mixture was incubated at 25 °C and was used to conduct periodic assays of the activity of TIM toward catalysis of isomerization of GAP. No significant loss of TIM activity was observed during any of these reactions that were followed for up to 7 days. The reactions in the absence of phosphite dianion were followed until they were 70–80% complete, and the reactions in the presence of phosphite dianion were typically followed until they were 40% complete, after which the protein was removed by ultrafiltration and the solution pD determined. There was no significant change in pD during any of these reactions.

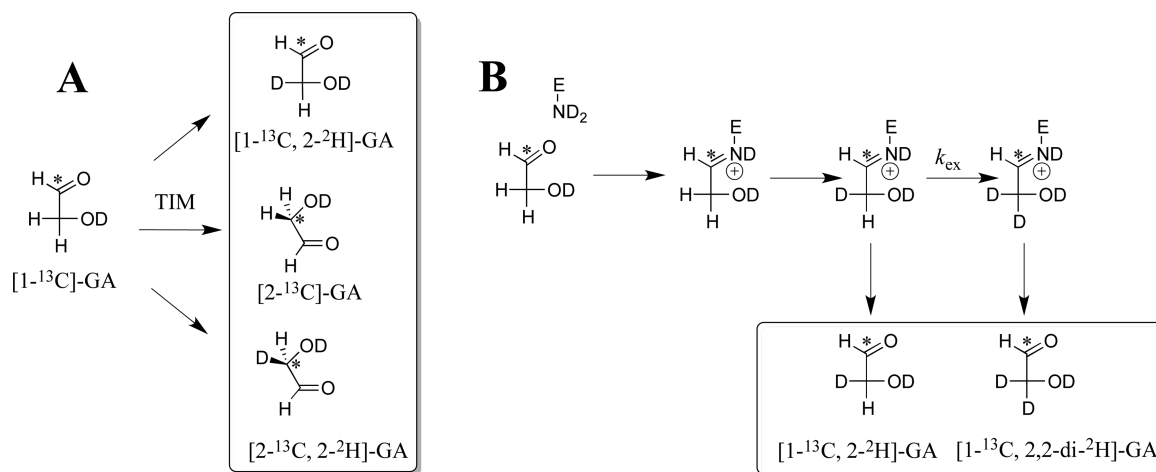
^1H NMR analyses of the products of these reactions were conducted by monitoring the signals for the hydrates of the products [$2\text{-}^{13}\text{C}$]GA, [$2\text{-}^{13}\text{C},2\text{-}^2\text{H}$]GA, [$1\text{-}^{13}\text{C},2\text{-}^2\text{H}$]GA, and

Table 1. Kinetic Parameters for Isomerization of GAP and DHAP Catalyzed by Wild-Type and Mutant Forms of Triosephosphate Isomerase from Chicken Muscle and *T. brucei brucei* at pH 7.5 and 25 °C^a

TIM	GAP ^b				DHAP ^c			
	k_{cat} (s ⁻¹)	K_m (mM)	k_{cat}/K_m (M ⁻¹ s ⁻¹)	K_i (mM) PGA ^d	k_{cat} (s ⁻¹)	K_m (mM)	k_{cat}/K_m (M ⁻¹ s ⁻¹)	K_i (mM) arsenate ^e
wild-type <i>c</i> TIM	3200 ± 100	0.29 ± 0.02	1.1 × 10 ⁷	0.019 ± 0.001	340 ± 5	0.59 ± 0.05	5.8 × 10 ⁵	9.6 ± 1.6
L7RM <i>c</i> TIM	16 ± 1	0.27 ± 0.02	5.9 × 10 ⁴	2.3 ± 0.1	8.0 ± 0.5	4.0 ± 0.2	2.0 × 10 ³	3.8 ± 0.3
wild-type <i>Tbb</i> TIM ^f	2100	0.25	8.4 × 10 ⁶	0.055 ^g	300	0.70	4.3 × 10 ⁵	4.6
P168A <i>Tbb</i> TIM	24 ± 1	0.091 ± 0.005	2.6 × 10 ⁵	0.14 ± 0.01	6.5 ± 0.1	0.49 ± 0.02	1.3 × 10 ⁴	10 ± 1

^aUnder standard assay conditions of 30 mM triethanolamine buffer at pH 7.5, 25 °C, and an ionic strength of 0.1 (NaCl). The kinetic parameters have been calculated using the total concentration of the free carbonyl and hydrated forms of GAP or DHAP. ^bThe errors for TIM-catalyzed isomerization of GAP were determined from the average of kinetic parameters determined in two experiments. ^cThe errors for TIM-catalyzed isomerization of DHAP are the standard deviations determined from the nonlinear least-squares fits of the kinetic data. ^dThe initial velocity of the isomerization of several concentrations of GAP was determined in the presence of 0.021 and 0.053 mM PGA for wild-type *c*TIM, 1.9 and 4.9 mM PGA for L7RM *c*TIM, and 0.13 and 0.39 mM PGA for P168A *Tbb*TIM. ^eThe initial velocity of the isomerization of several concentrations of DHAP was determined in the presence of 2, 5, and 10 mM arsenate. ^fData from ref 54, unless noted otherwise. ^gFrom ref 19.

Scheme 2



[1-¹³C,2,2-di-²H]GA, and the fractional yields of these products, f_p , were determined at several times during the first 20–40% of the reaction, as described previously.⁴⁹ Observed first-order rate constants for the disappearance of [1-¹³C]GA, k_{obs} (s⁻¹), were determined from the slopes of linear semilogarithmic plots of reaction progress against time covering the first 30–40% of the reaction, according to eq 1

$$\ln f_s = -k_{\text{obs}}t \tag{1}$$

where f_s is the fraction of [1-¹³C]GA remaining at time t . The observed second-order rate constants for the disappearance of [1-¹³C]GA, $(k_{\text{cat}}/K_m)_{\text{obs}}$ (M⁻¹ s⁻¹), were calculated from the values of k_{obs} using eq 2

$$(k_{\text{cat}}/K_m)_{\text{obs}} = \frac{k_{\text{obs}}}{(1 - f_{\text{hyd}})[E]} \tag{2}$$

where f_{hyd} (=0.94) is the fraction of [1-¹³C]GA present in the unreactive hydrate form and $[E]$ is the concentration of TIM.³⁰

RESULTS

Kinetic Parameters and Inhibition Constants. Kinetic parameters k_{cat} and K_m for the isomerization of GAP catalyzed by wild-type *c*TIM, L7RM *c*TIM, and P168A *Tbb*TIM at pH 7.5, 25 °C, and an ionic strength of 0.1 (NaCl) were determined by Michaelis–Menten analyses of initial velocities and are reported in Table 1. Values of K_i for competitive

inhibition of these TIMs by 2-phosphoglycolate (PGA) were determined from the dependence of the initial velocity of isomerization of GAP at several concentrations of GAP at two different fixed concentrations of PGA. These values of K_i (Table 1) were obtained from the nonlinear least-squares fit of the initial velocity data to eq 3, where $[I] = [\text{PGA}]$, and using the values of K_m listed in Table 1. Arsenate is an activator of glyceraldehyde-3-phosphate dehydrogenase, which was used as the coupling enzyme in assays of the TIM-catalyzed isomerization of DHAP to give GAP.^{20,50} The initial velocity of the isomerization of several concentrations of DHAP catalyzed by wild-type *c*TIM, L7RM *c*TIM, and P168A *Tbb*TIM at pH 7.5, 25 °C, and an ionic strength of 0.1 (NaCl) was determined in the presence of 2, 5, and 10 mM arsenate. Values of k_{cat} and K_m for the isomerization of DHAP, along with values of K_i for arsenate, were obtained from the nonlinear least-squares fit of the initial velocity data to a modified form of eq 3

$$\frac{v_i}{[E]} = \frac{k_{\text{cat}}[\text{GAP}]}{[\text{GAP}] + K_m(1 + [I]/K_i)} \tag{3}$$

where $[I] = [\text{arsenate}]$ for the substrate DHAP, and are reported in Table 1.

TIM-Catalyzed Reactions of [1-¹³C]GA in D₂O. The disappearance of the substrate and the formation of the four identifiable products, shown in the boxes in Scheme 2, from the reaction of the truncated neutral substrate [1-¹³C]GA catalyzed

by wild-type *c*TIM, L7RM *c*TIM, and P168A *Tbb*TIM in D₂O buffered by 20 mM imidazole at pD 7.0, 25 °C, and an ionic strength of 0.1 (NaCl) were monitored by ¹H NMR spectroscopy for up to 7 days, as described previously.^{20,49} The fractional yields of products [2-¹³C]GA, [2-¹³C,2-²H]GA, [1-¹³C,2-²H]GA, and [1-¹³C,2,2-di-²H]GA, f_p , were determined by ¹H NMR analysis at five different times during the disappearance of the first 20–40% of [1-¹³C]GA, as described previously.^{20,49} The observed first-order rate constants for the disappearance of [1-¹³C]GA in these reactions, k_{obs} (s⁻¹), were determined as the slopes of semilogarithmic plots of reaction progress versus time, according to eq 1. The observed second-order rate constants for the disappearance of [1-¹³C]GA, $(k_{cat}/K_m)_{obs}$ (M⁻¹ s⁻¹), were calculated from the values of k_{obs} using eq 2.

Wild-Type *c*TIM-Catalyzed Reactions of [1-¹³C]GA in D₂O. The relatively rapid phosphite-activated reactions of [1-¹³C]GA catalyzed by wild-type *c*TIM in D₂O in the presence of ≥2.0 mM HPO₃²⁻ result in essentially quantitative conversion of the substrate to the three products shown in Scheme 2A: [2-¹³C]GA, [2-¹³C,2-²H]GA, and [1-¹³C,2-²H]GA (Table S1 of the Supporting Information).⁴⁹ By contrast, the very slow unactivated reaction of [1-¹³C]GA in the presence of wild-type *c*TIM gives the three products observed for the phosphite-activated reaction (Scheme 2A), along with a significant 19% yield of [1-¹³C,2,2-di-²H]GA that forms in a nonspecific protein-catalyzed reaction that occurs outside the active site of TIM (Scheme 2B), and the total yield of the four identifiable products is only ~60% (Table S1 of the Supporting Information).⁴⁹ We proposed previously that [1-¹³C,2,2-di-²H]GA forms by a slow protein-catalyzed reaction that involves deuterium exchange into [1-¹³C]GA catalyzed by the amine side chains of surface lysine residues (Scheme 2B).⁵³ The absolute fractional yields of the products of the unactivated and phosphite dianion-activated wild-type *c*TIM-catalyzed reactions, f_p , are reported in Table S1 of the Supporting Information. There is good agreement between the fractional product yields from the phosphite dianion-activated reactions determined here and those reported previously.⁴⁹ However, the normalized yields of 45% [2-¹³C,2-²H]GA and 42% [1-¹³C,2-²H]GA (Table S1 of the Supporting Information) from the specific reaction of [1-¹³C]GA at the active site of wild-type *c*TIM determined here are smaller and larger, respectively, than those of 60 and 30% reported previously.⁴⁹ We conclude that, in our hands, the uncertainty in the yields of the products of the unactivated wild-type *c*TIM-catalyzed reactions of [1-¹³C]GA is larger than that for the phosphite dianion-activated reactions. These unactivated reactions of [1-¹³C]GA in the presence of TIM are very slow, were monitored for several days, and give only low yields of [2-¹³C,2-²H]GA and [1-¹³C,2-²H]GA (Table S1 of the Supporting Information). In addition, the signals of the multiplet due to the C-2 proton of [1-¹³C,2-²H]GA are not fully resolved from the very large doublet due to the C-2 proton of the substrate [1-¹³C]GA, which complicates the reliable determination of the yield of this product.⁴⁹

Table S1 of the Supporting Information gives the true second-order rate constants, k_{cat}/K_m (M⁻¹ s⁻¹), for the wild-type *c*TIM-catalyzed reaction of the carbonyl form of [1-¹³C]GA to give the specific products of the TIM-catalyzed reaction [2-¹³C]GA, [2-¹³C,2-²H]GA, and [1-¹³C,2-²H]GA (Scheme 2A). For the reactions in the presence of phosphite,

these were calculated from the observed second-order rate constants $(k_{cat}/K_m)_{obs}$ using eq 4

$$\frac{k_{cat}}{K_m} = \left(\frac{k_{cat}}{K_m} \right)_{obs} \sum (f_p)_E \quad (4)$$

with $\sum (f_p)_E = 1.0$, where $\sum (f_p)_E$ is the sum of the fractional yields of these specific products. A second-order rate constant k_{cat}/K_m of 0.1 M⁻¹ s⁻¹ for the unactivated reaction in the absence of phosphite dianion was calculated using eq 4 with a $(k_{cat}/K_m)_{obs}$ of 0.19 M⁻¹ s⁻¹ and a $\sum (f_p)_E$ of 0.5 reported previously.⁴⁹

Figure 1A shows the dependence of k_{cat}/K_m (M⁻¹ s⁻¹) for wild-type *c*TIM-catalyzed reactions of [1-¹³C]GA on the

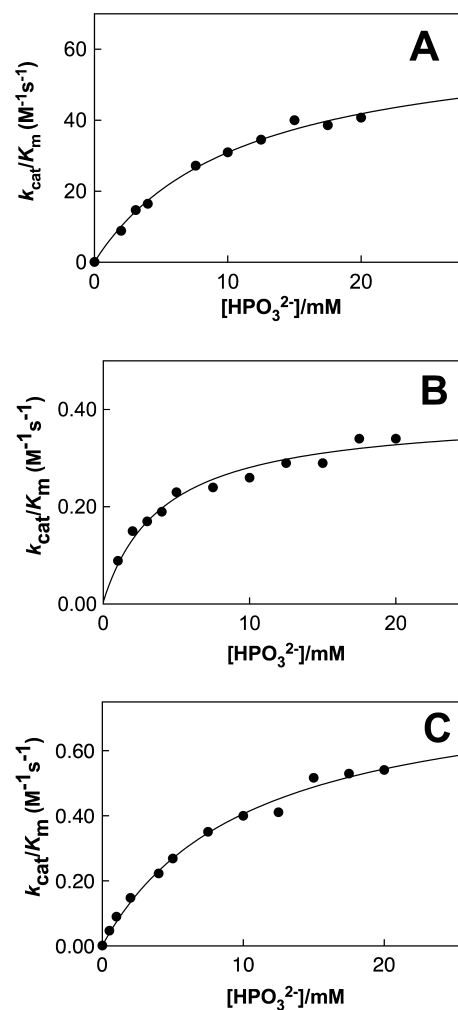
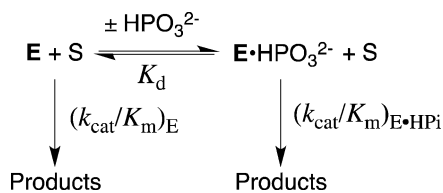


Figure 1. Dependence of the second-order rate constants k_{cat}/K_m for the TIM-catalyzed turnover of the free carbonyl form of [1-¹³C]GA in D₂O on $[HPO_3^{2-}]$ at pD 7.0, 25 °C, and an ionic strength of 0.1 (NaCl). The data were fit to eq 5 derived for the model shown in Scheme 3: (A) wild-type *c*TIM, (B) L7RM *c*TIM, and (C) P168A *Tbb*TIM.

concentration of added phosphite dianion (HPO₃²⁻).³⁰ The solid line shows the nonlinear least-squares fit of these data to eq 5, derived for Scheme 3 ($S = [1-^{13}C]GA$), with $(k_{cat}/K_m)_E = 0.1$ M⁻¹ s⁻¹ for the unactivated reaction in the absence of phosphite. The data give a $(k_{cat}/K_m)_{E,HP}$ of 65 M⁻¹ s⁻¹ for turnover of [1-¹³C]GA by the phosphite-ligated enzyme and a

Scheme 3



K_d of 11 mM for binding of phosphite dianion to the free enzyme (Table 3).³⁰ Table 3 also gives the corresponding kinetic parameters for the reactions of [1-¹³C]GA catalyzed by wild-type *Tbb*TIM that were determined previously.⁵⁴

$$\begin{aligned}
 k_{\text{cat}}/K_m = & \left(\frac{K_d}{K_d + [\text{HPO}_3^{2-}]} \right) (k_{\text{cat}}/K_m)_E \\
 & + \left(\frac{[\text{HPO}_3^{2-}]}{K_d + [\text{HPO}_3^{2-}]} \right) (k_{\text{cat}}/K_m)_{\text{E} \cdot \text{HPi}} \quad (5)
 \end{aligned}$$

L7RM cTIM-Catalyzed Reactions of [1-¹³C]GA in D₂O.

The 208-TGAG for 208-YGGs loop 7 replacement mutation of cTIM results in a decrease in the midpoint for thermal denaturation from 60 °C for the wild type to 49 °C for L7RM cTIM.²⁸ However, despite this, we find that L7RM cTIM maintains full catalytic activity over a period of 7 days during the reaction of 20 mM [1-¹³C]GA at pD 7.0, 25 °C, and an ionic strength of 0.1 (NaCl).

Table S2 of the Supporting Information gives the fractional yields of the four identifiable products from the unactivated and phosphite dianion-activated L7RM cTIM-catalyzed reactions of [1-¹³C]GA that are shown in Scheme 2. The major product of the unactivated reaction of [1-¹³C]GA in the absence of phosphite dianion is [1-¹³C,2,2-di-²H]GA, which is formed in a yield of 27% by the nonspecific protein-catalyzed reaction shown in Scheme 2B. The very small yields of 1.5%

[2-¹³C,2-²H]GA and ~0.2% [2-¹³C]GA show that L7RM cTIM maintains only a low activity for catalysis of the reactions of [1-¹³C]GA at the enzyme active site (Scheme 2A).⁵³ The observed yield of 3.3% [1-¹³C,2-²H]GA is formed by both the specific reaction shown in Scheme 2A and the nonspecific reaction shown in Scheme 2B. A yield of ~1.1% [1-¹³C,2-²H]GA from only the specific reaction was estimated with the assumption that the ratio of the yields of [1-¹³C,2-²H]GA and [2-¹³C,2-²H]GA from the unactivated reaction is the same as that for the phosphite-activated reactions (see Table S2 of the Supporting Information).

Table 2 gives the observed second-order rate constants (k_{cat}/K_m)_{obs} for the L7RM cTIM-catalyzed reactions of [1-¹³C]GA and the true second-order rate constants k_{cat}/K_m for the specific reactions at the active site of L7RM cTIM that were calculated from the values of (k_{cat}/K_m)_{obs} using eq 4 with the values of $\sum(f_p)$ listed in Table 2, where $\sum(f_p)_E$ is the sum of the fractional yields of these specific products (Table S2 of the Supporting Information).

Figure 1B shows the dependence of k_{cat}/K_m (M⁻¹ s⁻¹) for the L7RM cTIM-catalyzed reactions of [1-¹³C]GA on the concentration of added phosphite dianion (HPO₃²⁻).³⁰ The solid line shows the nonlinear least-squares fit of these data to eq 5, with a (k_{cat}/K_m)_E of 0.0045 M⁻¹ s⁻¹ for the unactivated reaction in the absence of phosphite (Table 2). The data give a (k_{cat}/K_m)_{E·HPi} of 0.39 M⁻¹ s⁻¹ for turnover of [1-¹³C]GA by the phosphite-liganded enzyme, and $K_d = 4.1$ mM for binding of phosphite dianion to the free enzyme (Table 3).³⁰ The upper limit for (k_{cat}/K_m)_E, calculated using eq 4 with the assumption that [1-¹³C,2-²H]GA forms exclusively by the specific pathway shown in Scheme 2A, is ≤0.008 M⁻¹ s⁻¹.

P168A TbbTIM-Catalyzed Reactions of [1-¹³C]GA in D₂O. Table S3 of the Supporting Information gives the fractional yields of the four identifiable products from the unactivated and phosphite dianion-activated P168A *Tbb*TIM-

Table 2. Second-Order Rate Constants for the Reactions of [1-¹³C]GA in D₂O Catalyzed by L7RM cTIM and P168A TbbTIM in the Absence and Presence of Phosphite Dianion in D₂O at 25 °C^a

L7RM cTIM					P168A TbbTIM				
[HPO ₃ ²⁻] (mM)	[TIM] (mM)	$\sum(f_p)_E^b$	(k_{cat}/K_m) _{obs} ^c (M ⁻¹ s ⁻¹)	(k_{cat}/K_m) ^d (M ⁻¹ s ⁻¹)	[HPO ₃ ²⁻] (mM)	[TIM] (mM)	$\sum(f_p)_E^b$	(k_{cat}/K_m) _{obs} ^c (M ⁻¹ s ⁻¹)	(k_{cat}/K_m) ^d (M ⁻¹ s ⁻¹)
0	0.48	0.03 ^e	0.15	0.0045	0	0.22	0.02 ^e	0.07	0.0014
1.0	0.34	0.37	0.24	0.089	0	0.49	0.02 ^e	0.06	0.0012
2.0	0.52	0.64	0.24	0.15	0.5	0.35	0.43	0.11	0.047
3.0	0.37	0.59	0.28	0.17	1.0	0.30	0.60	0.15	0.090
4.0	0.24	0.59	0.32	0.19	2.0	0.25	0.70	0.21	0.15
5.0	0.21	0.59	0.39	0.23	4.0	0.20	0.65	0.34	0.22
7.5	0.30	0.61	0.40	0.24	5.0	0.12	0.71	0.38	0.27
10	0.17	0.65	0.40	0.26	7.5	0.12	0.70	0.50	0.35
13	0.14	0.61	0.47	0.29	10	0.080	0.71	0.57	0.40
15	0.15	0.62	0.46	0.29	13	0.070	0.66	0.62	0.41
18	0.10	0.63	0.54	0.34	15	0.060	0.67	0.77	0.52
20	0.090	0.61	0.56	0.34	18	0.060	0.70	0.75	0.53
20	0.10	0.59	0.58	0.34	20	0.14	0.80	0.68	0.54

^aDetermined by ¹H NMR analysis of the reaction of 20 mM [1-¹³C]GA in D₂O at pD 7.0 (20 mM imidazole), 25 °C, and an ionic strength of 0.1 (NaCl). ^bThe sum of the yields of the specific products [2-¹³C]GA, [2-¹³C,2-²H]GA, and [1-¹³C,2-²H]GA from the reaction of [1-¹³C]GA at the enzyme active site (Scheme 2A), taken from Tables S2 and S3 of the Supporting Information. ^cObserved second-order rate constant for the TIM-catalyzed reactions of [1-¹³C]GA, calculated from the observed first-order rate constant using eq 2. ^dSecond-order rate constant for the specific TIM-catalyzed reaction of [1-¹³C]GA to give the products shown in Scheme 2A, calculated from (k_{cat}/K_m)_{obs} for the disappearance of [1-¹³C]GA using eq 4. ^eCalculated using the estimated yield of [1-¹³C,2-²H]GA formed by the specific reaction shown in Scheme 2A listed in Tables S2 and S3 of the Supporting Information.

Table 3. Kinetic Parameters for the Unactivated and Phosphite-Activated Reactions of the Free Carbonyl Form of [1-¹³C]GA Catalyzed by Wild-Type and Mutant Forms of Triosephosphate Isomerase from Chicken Muscle and *T. brucei brucei* in D₂O at 25 °C (Scheme 3)^a

TIM	$(k_{\text{cat}}/K_m)_E^b$ (M ⁻¹ s ⁻¹)	$(k_{\text{cat}}/K_m)_{E\cdot\text{HP}_i}^c$ (M ⁻¹ s ⁻¹)	K_d^d (mM)	$K_d^{\ddagger e}$ (mM)	$(k_{\text{cat}}/K_m)_{E\cdot\text{HP}_i}/(k_{\text{cat}}/K_m)_E$	$(k_{\text{cat}}/K_m)_{E\cdot\text{HP}_i}/K_d^f$ (M ⁻² s ⁻¹)
wild-type <i>c</i> TIM	0.1 ^g	65 ± 4	11 ± 1.3	0.017	650	5900
L7RM <i>c</i> TIM	0.0045 (<0.008) ^h	0.39 ± 0.02	4.1 ± 0.5	0.042	100	95
wild-type <i>Tbb</i> TIM ⁱ	0.07	64	19	0.021	900	3400
P168A <i>Tbb</i> TIM	0.0013 (<0.01) ^h	0.83 ± 0.05	10 ± 1.3	0.016	600	83

^aDetermined by ¹H NMR analysis of the reaction of 20 mM [1-¹³C]GA in D₂O at pD 7.0 (20 mM imidazole), 25 °C, and an ionic strength of 0.1 (NaCl). ^bSecond-order rate constant for the unactivated TIM-catalyzed reaction of [1-¹³C]GA in the absence of phosphite dianion. ^cSecond-order rate constant for the reaction of [1-¹³C]GA catalyzed by the phosphite-liganded enzyme. ^dDissociation constant for binding of phosphite dianion to the free enzyme. ^eDissociation constant for release of phosphite dianion from the transition state complex, calculated using eq 6 derived for Scheme 4. ^fThird-order rate constant for the phosphite-activated TIM-catalyzed reaction of [1-¹³C]GA. ^gCalculated from data reported in ref 49 (see Table S1 of the Supporting Information). ^hUpper limit for $(k_{\text{cat}}/K_m)_E$ calculated using eq 4 with the assumption that [1-¹³C,2-²H]GA forms exclusively by the specific pathway shown in Scheme 2A. ⁱData from ref 54.

catalyzed reactions of [1-¹³C]GA that are shown in Scheme 2. The major product of the unactivated reaction of [1-¹³C]GA in the absence of phosphite dianion is [1-¹³C,2,2-di-²H]GA, which is formed in a yield of 33% by the nonspecific protein-catalyzed pathway shown in Scheme 2B. There is only a small yield of 1.0% [2-¹³C,2-²H]GA and no detectable formation of [2-¹³C]GA. The observed yield of 11% [1-¹³C,2-²H]GA from both the specific reaction shown in Scheme 2A and the nonspecific reaction shown in Scheme 2B is substantially larger than the 3.3% yield of this product from the corresponding L7RM *c*TIM-catalyzed reaction, but similar to the 10% yield observed for the reaction catalyzed by a monomeric variant of *Tbb*TIM, for which there is no detectable activation by phosphite dianion.⁵⁴ These results are consistent with a relatively high activity of *Tbb*TIM for catalysis of deuterium exchange by the nonspecific pathway shown in Scheme 2B. *Tbb*TIM has an isoelectric point of 9.8,⁵⁵ which is 3–4 units higher than that for the TIMs from yeast⁵⁵ and rabbit muscle.⁵⁵ We suggest that the greater reactivity of *Tbb*TIM in the pathway shown in Scheme 2B reflects a relatively large surface density of the amine side chains of lysine residues. A yield of ~1% [1-¹³C,2-²H]GA from only the specific reaction was estimated with the assumption that the ratio of the yields of [1-¹³C,2-²H]GA and [2-¹³C,2-²H]GA from the unactivated reaction is the same as that for the phosphite-activated reactions (see Table S3 of the Supporting Information).

Table 2 gives the observed second-order rate constants, $(k_{\text{cat}}/K_m)_{\text{obs}}$, for the P168A *Tbb*TIM-catalyzed reactions of [1-¹³C]GA and the true second-order rate constants, k_{cat}/K_m , for the specific reactions at the active site of P168A *Tbb*TIM that were calculated from the values of $(k_{\text{cat}}/K_m)_{\text{obs}}$ using eq 4 with the values of $\sum(f_p)$ listed in Table 2, where $\sum(f_p)_E$ is the sum of the fractional yields of these specific products (Table S3 of the Supporting Information).

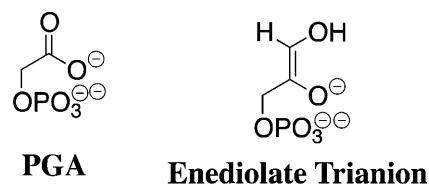
Figure 1C shows the dependence of k_{cat}/K_m (M⁻¹ s⁻¹) for the P168A *Tbb*TIM-catalyzed reactions of [1-¹³C]GA on the concentration of added phosphite dianion (HPO₃²⁻).³⁰ The solid line shows the nonlinear least-squares fit of these data to eq 5, with a $(k_{\text{cat}}/K_m)_E$ of 0.0013 M⁻¹ s⁻¹ for the unactivated reaction in the absence of phosphite (Table 2). The data give a $(k_{\text{cat}}/K_m)_{E\cdot\text{HP}_i}$ of 0.83 M⁻¹ s⁻¹ for turnover of [1-¹³C]GA by the phosphite-liganded enzyme, and $K_d = 10$ mM for binding of phosphite dianion to the free enzyme (Table 3).³⁰ The upper limit for $(k_{\text{cat}}/K_m)_E$, calculated using eq 4 with the assumption that [1-¹³C,2-²H]GA forms exclusively by the specific pathway shown in Scheme 2A, is ≤0.01 M⁻¹ s⁻¹.

DISCUSSION

The TIMs from *T. brucei brucei* (*Tbb*TIM) and chicken muscle (*c*TIM) exhibit 50% sequence identity,⁵⁶ and the active site structures determined for complexes of these two TIMs with phosphoglycolohydroxamate (PGH) are nearly superimposable.^{54,57,58} No significant differences in the mechanism of action of TIM from these two sources have been observed,⁵⁹ and the mechanistic conclusions from studies of TIM from different organisms have been broadly generalized to all TIMs, except perhaps the enzymes from archaea.^{28,29}

The kinetic parameters for wild-type and mutant TIMs determined here (Table 1) are in agreement with those reported previously.^{28,41,60} The P168A mutation of *Tbb*TIM and the loop 7 replacement mutation of *c*TIM result in 30- and 190-fold decreases, respectively, in k_{cat}/K_m for catalysis of isomerization of GAP, which are due largely to the effects of these mutations on k_{cat} (Table 1). The loop 7 replacement mutant of *c*TIM results in a 120-fold increase in K_i for competitive inhibition by 2-phosphoglycolate (PGA) at pH 7.5. PGA is an early example of a tight-binding enzyme inhibitor that was proposed to be an analogue of the enediolate-like transition state for the catalyzed reaction (Chart 1).^{61–63} The

Chart 1

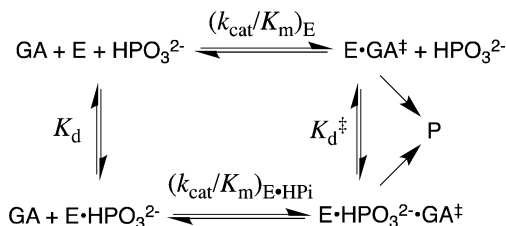


observation that the loop 7 replacement mutation results in similar large changes in k_{cat}/K_m for isomerization of GAP and DHAP and in K_i for inhibition by PGA shows that this mutation weakens, to a similar extent, interactions that stabilize the TIM-PGA complex and the transition state for isomerization. By contrast, the P168A mutation of *Tbb*TIM results in only a 2.5-fold increase in K_i for inhibition by PGA, which is significantly smaller than the 30-fold effect of this mutation on k_{cat}/K_m for the *Tbb*TIM-catalyzed isomerization of GAP. This shows that the P168A mutation affects interactions that control the barrier for formation of the enzyme-bound transition state but do not strongly stabilize the TIM-PGA complex.

Reactions of Substrate Pieces. We have characterized the activation of wild-type and mutant TIM-catalyzed reactions of

the truncated neutral substrate glycolaldehyde (GA) by phosphite dianion in terms of three kinetic parameters (Scheme 4): (1) the second-order rate constant, $(k_{\text{cat}}/K_m)_E$, for the

Scheme 4



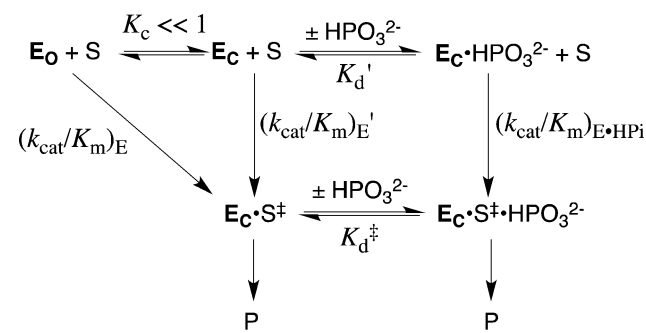
unactivated reaction catalyzed by the free enzyme in the absence of phosphite, (2) the second-order rate constant, $(k_{\text{cat}}/K_m)_{\text{E} \cdot \text{HPi}}$, for the reaction catalyzed by the binary $\text{E} \cdot \text{HPO}_3^{2-}$ complex, and (3) the dissociation constant, K_d , for breakdown of the $\text{E} \cdot \text{HPO}_3^{2-}$ complex, which measures the affinity of the free enzyme for phosphite dianion. Additionally, the dissociation constant for release of phosphite from the transition state, K_d^\ddagger (Scheme 4), which is a measure of the intrinsic phosphite binding energy, may then be calculated from these three experimental parameters according to eq 6. Table 3 summarizes these parameters for the wild-type and mutant TIM studied here, along with the third-order rate constants, $(k_{\text{cat}}/K_m)_{\text{E} \cdot \text{HPi}}/K_d$ ($\text{M}^{-2} \text{s}^{-1}$), for the reactions of the two-part substrate GA with phosphite.

$$K_d^\ddagger = \frac{K_d(k_{\text{cat}}/K_m)_E}{(k_{\text{cat}}/K_m)_{\text{E} \cdot \text{HPi}}} \quad (6)$$

The P168A mutation of *Tbb*TIM results in similar 30- and 40-fold decreases, respectively, in second-order rate constant k_{cat}/K_m (Table 1) for the reaction of the whole substrate GAP and third-order rate constant $(k_{\text{cat}}/K_m)_{\text{E} \cdot \text{HPi}}/K_d$ (Table 3) for the reaction of the substrate pieces GA and phosphite, while the loop 7 replacement mutation of *c*TIM results in a slightly larger 190-decrease in k_{cat}/K_m for GAP and a 60-fold decrease in $(k_{\text{cat}}/K_m)_{\text{E} \cdot \text{HPi}}/K_d$ for the pieces. We conclude that these quite different structural mutations result in a similar loss of stabilizing interactions between the protein and the transition state for the enzyme-catalyzed reaction of both the whole substrate GAP and the substrate pieces GA and HPO_3^{2-} . These results add to a large body of data that are consistent with the conclusion that the primary effect of covalent connections between substrate pieces,^{20,30–32,34,64–66} or in some cases enzyme pieces,^{17,67} is to reduce the unfavorable entropic barrier associated with the reaction of the pieces, relative to that for the reaction of the whole substrate or enzyme.⁶⁸

The well-documented phosphodianion-driven conformational change of TIM has been incorporated into the model shown in Scheme 5, which rationalizes the activation of the enzyme by the binding of HPO_3^{2-} .^{20,21,49} In this model, TIM exists in a dominant loop open enzyme form E_O that is inactive and a rare, higher-energy but active, loop-closed enzyme form E_C [$K_c \ll 1$ (Scheme 5)]. A large fraction of the free energy barrier for the conversion of E_O to E_C may represent the barrier to desolvation of the enzyme active site that accompanies ligand binding and loop closure.^{18,37} The loop-closed form shows specificity for binding of both HPO_3^{2-} and the transition state for the reaction of the substrate piece, GA^\ddagger . The overall binding

Scheme 5



affinity of HPO_3^{2-} and of the transition state GA^\ddagger for free TIM is relatively weak, because a substantial portion of the ligand binding energy is used to drive the transformation from inactive E_O to active E_C in forming the binary $\text{E}_C \cdot \text{HPO}_3^{2-}$ or $\text{E}_C \cdot \text{GA}^\ddagger$ complex (Scheme 5). By contrast, the full intrinsic binding energy of the second ligand is observed upon conversion of these binary complexes of the ternary $\text{E}_C \cdot \text{HPO}_3^{2-} \cdot \text{GA}^\ddagger$ complex. We use Scheme 5 as the framework for our discussion of structure–reactivity relationships for the P168A and loop 7 replacement mutations of TIM.

P168A Mutation. Figure 2 shows the X-ray crystal structures in the active site region of unliganded wild-type

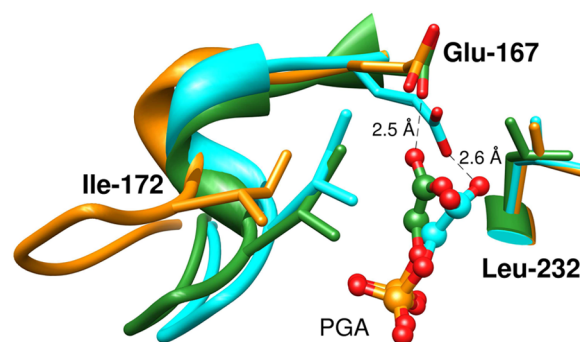


Figure 2. Superposition of models, from X-ray crystal structures, which show the active sites of unliganded wild-type *Tbb*TIM (gold, PDB entry 5TIM), PGA-liganded TIM from *L. mexicana* (cyan, PDB entry 1N55), and PGA-liganded P168A mutant *Tbb*TIM (green, PDB entry 2J27). The ligand-induced enzyme conformational changes observed for wild-type and P168A *Tbb*TIM are similar, except that the carboxylate side chain of Glu167 remains in an open swung-out conformation in the P168A mutant.

*Tbb*TIM (gold, 2.1 Å resolution),⁶⁹ PGA-liganded wild-type TIM from *Leishmania mexicana* (cyan, 0.83 Å resolution),⁷⁰ and PGA-liganded P168A mutant *Tbb*TIM (green, 1.15 Å resolution).⁴¹ A comparison of the X-ray crystal structures for unliganded wild-type and P168A mutant *Tbb*TIM shows that the mutation causes only small changes in protein structure.⁴¹ The binding of PGA to wild-type TIM (Figure 2, gold) triggers the large conformational change to give the loop-closed enzyme (Figure 2, green).⁴¹ This movement of loop 6 from the open to the closed conformation is accompanied by 90° and 180° rotations in the planes defined by the peptide bonds of Gly211 and Gly212, respectively, which results in a steric clash between the carbonyl oxygen of Gly211 and the pyrrolidine side chain of Pro168.⁶⁹ This strain is relieved by movement of the pyrrolidine ring of Pro168 that “swings” the neighboring carboxylate side

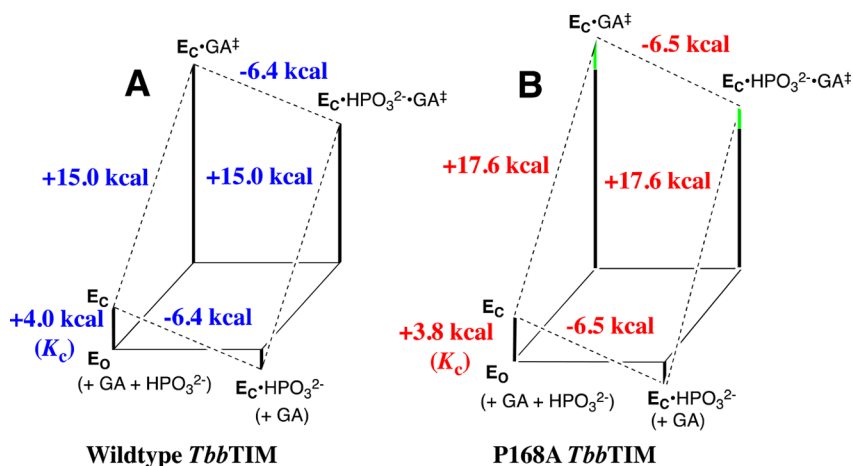


Figure 3. Free energy profiles for turnover of GA by free TIM (E_O) and by TIM that is saturated with HPO_3^{2-} ($E_C \cdot HPO_3^{2-}$), constructed for Scheme 5 using the kinetic parameters listed in Table 3. The profiles show the activation free energy changes calculated using the Eyring equation at 298 K for reactions catalyzed by wild-type and P168A mutant *TbbTIM*. (A) Reactions catalyzed by wild-type ϵ TIM. The difference between the total intrinsic phosphite dianion binding energy of -6.4 kcal/mol and the ΔG° of -2.4 kcal/mol for binding of HPO_3^{2-} to inactive open enzyme E_O to give active closed liganded enzyme $E_C \cdot HPO_3^{2-}$ is attributed to the ΔG_C of 4.0 kcal/mol for the conformational change that converts E_O to E_C . (B) Reactions catalyzed by the P168A mutant. The observed barriers for conversion of E_O to the transition state for the unactivated and phosphite dianion-activated reaction are 2.6 kcal/mol higher than for the wild-type ϵ TIM-catalyzed reaction (green bars).

chain of the active site base Glu167 toward the PGA ligand.^{41,69} Figure 2 shows that the binding of PGA to the P168A mutant of *TbbTIM* triggers nearly the same conformational change as that observed for wild-type TIM. However, the effect of replacement of the cyclic pyrrolidine side chain with the smaller methyl group at position 168 is to remove the steric clash with the mobile carbonyl oxygen of Gly211, so that the side chain of Glu167 remains in the “swung out” position that is observed for unliganded open wild-type TIM.⁴¹ PGA binds, formally, as the trianion to TIM, and this binding is accompanied by the uptake of a proton by Glu167 that results in the formation of a hydrogen bond between the carboxyl groups of bound PGA and Glu167.¹⁹ The P168A mutation of *TbbTIM* results in movement of the PGA ligand toward the nearly stationary side chain of Glu167. This preserves the ligand–side chain hydrogen bond (Figure 2) and so may provide a rationalization for the small effect of the mutation on K_i for inhibition by PGA (Table 1).

Panels A and B of Figure 3 show free energy diagrams, constructed for the model shown in Scheme 5, illustrating the effect of the P168A mutation of *TbbTIM* on the unactivated and phosphite-activated TIM-catalyzed reactions of GA. The free energies of activation were calculated from the kinetic parameters listed in Table 3 using the Eyring equation at 298 K, with the assumption that the phosphite dianion functions solely as a “spectator” to hold TIM in the active closed E_C form, so that $(k_{cat}/K_m)_{E'} = (k_{cat}/K_m)_{E \cdot HP_i}$ (Scheme 5).^{20,30} The free energy barrier to the unactivated wild-type enzyme-catalyzed reaction of GA, calculated from $(k_{cat}/K_m)_{E'}$, can be partitioned into the barrier for the conformational change that converts inactive enzyme E_O to active enzyme E_C (given by $-RT \ln K_C$, eq 7), and the barrier to catalysis by the active closed enzyme $(k_{cat}/K_m)_{E'} = (k_{cat}/K_m)_{E \cdot HP_i}$ (Scheme 5).

$$\frac{1}{K_C} = \frac{(k_{cat}/K_m)_{E \cdot HP_i}}{(k_{cat}/K_m)_E} \quad (7)$$

The carboxylate anion side chain of Glu167 at the P168A mutant enzyme·PGA complex remains in the swung out

position, compared with the “swung in” position for wild-type *TbbTIM* (Figure 2). This structural change results in a 30-fold fold decrease in k_{cat}/K_m for the enzyme-catalyzed isomerization of GAP (Table 1), and 50- and 80-fold decreases in $(k_{cat}/K_m)_E$ and $(k_{cat}/K_m)_{E \cdot HP_i}$, respectively, for the deprotonation of GA by TIM and by the TIM· HPO_3^{2-} complex (Table 3). There is also almost no effect of the P168A mutation on the ratio of the second-order rate constants for the reactions of GA catalyzed by the free enzyme and the phosphite-liganded enzyme, $(k_{cat}/K_m)_{E \cdot HP_i}/(k_{cat}/K_m)_E$. This is consistent with an only small effect of this mutation on the equilibrium constant for the interconversion of the open inactive and closed active forms of the enzyme, K_C (eq 7), so that the change in $(k_{cat}/K_m)_E$ is due mainly to the change in $(k_{cat}/K_m)_{E'}$ \approx $(k_{cat}/K_m)_{E \cdot HP_i}$. Finally, there is almost no effect of the mutation on K_d^\ddagger for the binding of phosphite dianion to the transition state $E_C \cdot GA^\ddagger$ (Table 3), resulting in essentially identical intrinsic phosphite dianion binding energies of 6.4 and 6.5 kcal/mol for wild-type and P168A mutant *TbbTIM*, respectively (Figure 3).

The decreases in $(k_{cat}/K_m)_E$ and $(k_{cat}/K_m)_{E \cdot HP_i}$ observed for P168A mutant *TbbTIM* reflect the increases in the reaction barrier associated with the shift in the side chain of Glu167 away from its optimally aligned swung in position in the wild-type enzyme.⁷¹ The P168A mutation is not expected to alter protein–phosphodianion interactions, and we observe no effect of this mutation on the intrinsic phosphite binding energy (Figure 3). Calculations are consistent with the conclusion that the five-membered pyrrolidine ring of the side chain of Pro168 adopts a strained planar configuration at the complex between PGA and TIM from *L. mexicana*.^{70,72} The relief of this strain by excision of the pyrrolidine ring at the P168A mutant would be expected to stabilize active enzyme E_C relative to inactive enzyme E_O and result in an increase in K_C . However, our results can be rationalized by an only small effect of the mutation on K_C , as discussed above. The small effect of the P168A mutation on the relative barriers to $(k_{cat}/K_m)_E$ and $(k_{cat}/K_m)_{E \cdot HP_i}$ might reflect a compensating increase in K_C and a

decrease in $(k_{\text{cat}}/K_{\text{m}})_{\text{E}}$, but we can provide no simple rationalization for such compensating changes.

Loop 7 Replacement Mutation. The binding of the enediolate intermediate analogue PGH to ϵ TIM results in the formation of a stunning array of hydrogen bonding interactions with loop 7 (Figure 4).²⁷ These include (1) interloop H-bonds

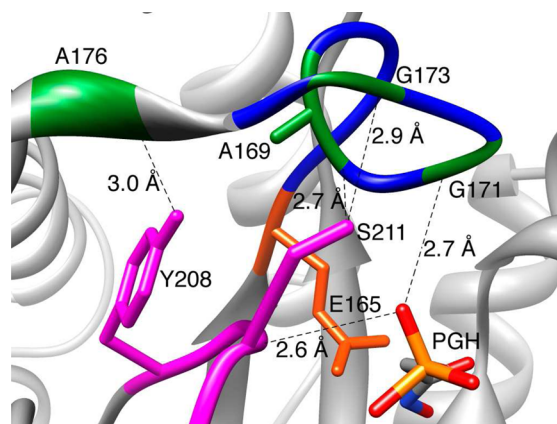


Figure 4. Representation of the structure of the closed form of TIM from chicken muscle in the region of the active site. This figure shows the important interactions between flexible loop 6 (Pro166–Ala176) and loop 7 (Tyr208–Ser211), which form upon binding of PGH, an analogue of the enediolate reaction intermediate (PDB entry ITPH).^{57,58} The 208-YGGG sequence was replaced by the 208-TGAG sequence in the loop 7 mutant of ϵ TIM. Reprinted from ref 27. Copyright 2010 Elsevier.

between (a) the backbone amide NH group of Gly173 from loop 6 and γ -O of Ser211 from loop 7, (b) the backbone amide NH group of Ala176 from loop 6 and the phenol oxygen of Try208 from loop 7, and (c) the carbonyl oxygen of Ala169 from loop 6 and the γ -OH group of Ser211 from loop 7 and (2) hydrogen bonds between the phosphodianion group of PGH and the backbone amide NH groups of Ser211.⁵⁸ This hydrogen bonding pattern has been perturbed by substitution of the YGGG motif at residues 208–211 with the 208-TGAG sequence commonly found in archaeal organisms.²⁸ Like the P168A mutation, this structural mutation results in significant decreases in $(k_{\text{cat}}/K_{\text{m}})_{\text{E-HP}_i}$ and $(k_{\text{cat}}/K_{\text{m}})_{\text{E}}$. Inspection of Figure 4 suggests that L7RM should have no effect on the important protein–phosphodianion interactions, so that no change in the intrinsic phosphite dianion binding energy is expected; only a small 2.5-fold increase in K_{d}^{\ddagger} is observed (Table 3).

The values of $(k_{\text{cat}}/K_{\text{m}})_{\text{E-HP}_i}$ and $(k_{\text{cat}}/K_{\text{m}})_{\text{E}}$ for L7RM ϵ TIM are 2-fold smaller and 3-fold larger, respectively, than the corresponding kinetic parameters for P168A mutant *Tbb*TIM (Table 3). This difference reflects the similar effects of the P168A mutation on $(k_{\text{cat}}/K_{\text{m}})_{\text{E-HP}_i}$ and $(k_{\text{cat}}/K_{\text{m}})_{\text{E}}$ discussed above, compared with the larger decrease in $(k_{\text{cat}}/K_{\text{m}})_{\text{E-HP}_i}$ relative to $(k_{\text{cat}}/K_{\text{m}})_{\text{E}}$ determined for L7RM of ϵ TIM. We propose that the P168A mutation has little effect on the magnitude of phosphite dianion activation of TIM-catalyzed reactions of GA, while the loop 7 replacement mutation results in a significant reduction in the level of dianion activation. These results are consistent with a 6.5-fold decrease in the value of $1/K_{\text{C}}$ (eq 7), from 650 for wild-type ϵ TIM to 100 for L7RM ϵ TIM (Table 3). This is consistent with the conclusion that the loop 7 replacement mutation results in a weakening of intra-

loop interactions that stabilize the active closed form of the enzyme.

Mechanism for Dianion Activation. The primary imperative for models for enzyme activation by HPO_3^{2-} is to provide a rationale for the specificity of phosphite dianion in binding to the transition state complex $\text{E}\cdot\text{GA}^{\ddagger}$ [K_{d}^{\ddagger} (Scheme 4)]. The specificity of closed enzyme E_{C} for binding both GA^{\ddagger} and HPO_3^{2-} (Scheme 5) provides for the tighter binding of HPO_3^{2-} to the transition state complex $\text{E}\cdot\text{GA}^{\ddagger}$ compared with the binding to the free enzyme that exists mainly as E_{O} (Figure 3). Selectivity in the binding of HPO_3^{2-} to the $\text{E}\cdot\text{GA}^{\ddagger}$ transition state complex might be the result of a direct stabilizing interaction between GA^{\ddagger} and phosphite dianion. We discount this possibility for the following reasons. First, the electrostatic interaction between phosphite dianion and the enolate–anion-like transition state for deprotonation of carbon is destabilizing. Second, only weak stabilizing intermolecular van der Waals interactions are expected for these small polar molecules. Third, only a single intermolecular hydrogen bond between the C-2 hydroxyl of GA and phosphite dianion is possible. However, inspection of X-ray crystal structures shows that the ligands adopt an extended conformation when bound to TIM (for example, see Figure 2). A stabilizing intermolecular hydrogen bond is unlikely to form at a transition state ternary complex $\text{E}\cdot\text{GA}\cdot\text{HPO}_3^{2-}$ that adopts a similar conformation.

The P168A and loop 7 replacement mutations of TIM result in an increase in the activation barriers to TIM-catalyzed deprotonation of GA, but little change in the intrinsic phosphite dianion binding energy. This result is consistent with a catalytic site at TIM that operates in a manner independent of the dianion activation site. The catalytic and activating sites must interact to the extent that dianion binding at the activator site triggers a conformational change that extends to the catalytic site. We propose for TIM (Scheme 5) that GA and HPO_3^{2-} bind essentially independently at the protein and that (a) the binding of HPO_3^{2-} at the dianion site plays the passive role of stabilizing the preexisting active enzyme E_{C} but does not affect the structure or intrinsic catalytic activity of E_{C} and (b) the binding of GA to E_{C} has little or no effect on the affinity of HPO_3^{2-} at the catalytic site. The result of the independent binding of the substrate pieces is to sequester GA at the catalytically active closed form of TIM. The binding loci for GA and HPO_3^{2-} lie essentially adjacent to one another at the active site for TIM, so that some structural mutations may affect the enzyme structure and function at both sites.

Finally, we note that mutations that affect the relative stability of E_{C} and E_{O} [K_{C} (Scheme 5)] may show complex effects on the kinetic parameters for catalysis of substrate deprotonation and on the magnitude of enzyme activation by phosphite dianion, as has been discussed in an earlier study of the L232A mutation of *Tbb*TIM.^{20,21} The data reported in this paper are consistent with a small 6.5-fold effect of L7RM on K_{C} that is reflected by the 6.5-fold decrease in the magnitude of the enzyme activation by phosphite dianion (Table 3).

■ ASSOCIATED CONTENT

📄 Supporting Information

Rate constants and fractional product yields for the reaction of [$1\text{-}^{13}\text{C}$]GA catalyzed by wild-type ϵ TIM (Table S1) and fractional product yields for the reaction of [$1\text{-}^{13}\text{C}$]GA catalyzed by the loop 7 replacement mutant of TIM from chicken muscle and the P168A mutant of *Tbb*TIM (Tables S2

and S3, respectively). This material is available free of charge via the Internet at <http://pubs.acs.org>.

AUTHOR INFORMATION

Corresponding Author

*E-mail: jrichard@buffalo.edu. Phone: (716) 645-4232. Fax: (716) 645-6963.

Funding

This work was supported by Grant GM 039754 from the National Institutes of Health.

Notes

The authors declare no competing financial interest.

ABBREVIATIONS

TIM, triosephosphate isomerase; *Tbb*TIM, TIM from *T. brucei brucei*; *c*TIM, TIM from chicken muscle; DHAP, dihydroxyacetone phosphate; GAP, (R)-glyceraldehyde 3-phosphate; GA, glycolaldehyde; PGA, 2-phosphoglycolate; PGH, phosphoglycolohydroxamate; L7RM, loop 7 replacement mutant; NADH, nicotinamide adenine dinucleotide, reduced form; NAD⁺, nicotinamide adenine dinucleotide, oxidized form; NMR, nuclear magnetic resonance; PDB, Protein Data Bank.

ADDITIONAL NOTE

^aWe note the following small differences in the numbering of amino acid residues at TIM from chicken muscle and TIM from *T. brucei brucei* (*c*TIM and *Tbb*TIM): Glu165 and Glu167, Pro166 and Pro168, Pro166–Ala176 and Pro168–Ala178 (loop 6), and Tyr208–Ser211 and Tyr210–Ser213 (loop 7), respectively.

REFERENCES

- (1) Knowles, J. R., and Albery, W. J. (1977) Perfection in enzyme catalysis: The energetics of triosephosphate isomerase. *Acc. Chem. Res.* 10, 105–111.
- (2) Knowles, J. R. (1991) To build an enzyme. *Philos. Trans. R. Soc., B* 332, 115–121.
- (3) Coulson, A. F. W., Knowles, J. R., Priddle, J. D., and Offord, R. E. (1970) Uniquely labeled active site sequence in chicken muscle triosephosphate isomerase. *Nature* 227, 180–181.
- (4) Hartman, F. C. (1970) Isolation and characterization of an active-site peptide from triosephosphate isomerase. *J. Am. Chem. Soc.* 92, 2170–2172.
- (5) Waley, S. G., Miller, J. C., Rose, I. A., and O'Connell, E. L. (1970) Identification of site in triosephosphate isomerase labeled by glycidol phosphate. *Nature* 227, 181.
- (6) Joseph-McCarthy, D., Rost, L. E., Komives, E. A., and Petsko, G. A. (1994) Crystal Structure of the Mutant Yeast Triosephosphate Isomerase in Which the Catalytic Base Glutamic Acid 165 Is Changed to Aspartic Acid. *Biochemistry* 33, 2824–2829.
- (7) Lodi, P. J., and Knowles, J. R. (1991) Neutral imidazole is the electrophile in the reaction catalyzed by triosephosphate isomerase: Structural origins and catalytic implications. *Biochemistry* 30, 6948–6956.
- (8) Komives, E. A., Chang, L. C., Lolis, E., Tilton, R. F., Petsko, G. A., and Knowles, J. R. (1991) Electrophilic catalysis in triosephosphate isomerase: The role of histidine-95. *Biochemistry* 30, 3011–3019.
- (9) Nickbarg, E. B., Davenport, R. C., Petsko, G. A., and Knowles, J. R. (1988) Triosephosphate isomerase: Removal of a putatively electrophilic histidine residue results in a subtle change in catalytic mechanism. *Biochemistry* 27, 5948–5960.
- (10) Gerlt, J. A., and Gassman, P. G. (1993) An Explanation for Rapid Enzyme-Catalyzed Proton Abstraction from Carbon Acids: Importance of Late Transition States in Concerted Mechanisms. *J. Am. Chem. Soc.* 115, 11552–11568.

- (11) Richard, J. P., and Amyes, T. L. (2001) Proton transfer at carbon. *Curr. Opin. Chem. Biol.* 5, 626–633.

- (12) Rieder, S. V., and Rose, I. A. (1959) Mechanism of the triosephosphate isomerase reaction. *J. Biol. Chem.* 234, 1007–1010.

- (13) O'Donoghue, A. C., Amyes, T. L., and Richard, J. P. (2005) Hydron Transfer Catalyzed by Triosephosphate Isomerase. Products of Isomerization of Dihydroxyacetone Phosphate in D₂O. *Biochemistry* 44, 2622–2631.

- (14) O'Donoghue, A. C., Amyes, T. L., and Richard, J. P. (2005) Hydron Transfer Catalyzed by Triosephosphate Isomerase. Products of Isomerization of (R)-Glyceraldehyde 3-Phosphate in D₂O. *Biochemistry* 44, 2610–2621.

- (15) Knowles, J. R. (1991) Enzyme catalysis: Not different, just better. *Nature* 350, 121–124.

- (16) Go, M. K., Koudelka, A., Amyes, T. L., and Richard, J. P. (2010) Role of Lys-12 in Catalysis by Triosephosphate Isomerase: A Two-Part Substrate Approach. *Biochemistry* 49, 5377–5389.

- (17) Go, M. K., Amyes, T. L., and Richard, J. P. (2010) Rescue of K12G Triosephosphate Isomerase by Ammonium Cations: The Reaction of an Enzyme in Pieces. *J. Am. Chem. Soc.* 132, 13525–13532.

- (18) Richard, J. P. (2012) A Paradigm for Enzyme-Catalyzed Proton Transfer at Carbon: Triosephosphate Isomerase. *Biochemistry* 51, 2652–2661.

- (19) Malabanan, M. M., Nitsch-Velasquez, L., Amyes, T. L., and Richard, J. P. (2013) Magnitude and Origin of the Enhanced Basicity of the Catalytic Glutamate of Triosephosphate Isomerase. *J. Am. Chem. Soc.* 135, 5978–5981.

- (20) Malabanan, M. M., Koudelka, A. P., Amyes, T. L., and Richard, J. P. (2012) Mechanism for Activation of Triosephosphate Isomerase by Phosphite Dianion: The Role of a Hydrophobic Clamp. *J. Am. Chem. Soc.* 134, 10286–10298.

- (21) Malabanan, M. M., Amyes, T. L., and Richard, J. P. (2011) Mechanism for Activation of Triosephosphate Isomerase by Phosphite Dianion: The Role of a Ligand-Driven Conformational Change. *J. Am. Chem. Soc.* 133, 16428–16431.

- (22) Pompliano, D. L., Peyman, A., and Knowles, J. R. (1990) Stabilization of a reaction intermediate as a catalytic device: Definition of the functional role of the flexible loop in triosephosphate isomerase. *Biochemistry* 29, 3186–3194.

- (23) Sampson, N. S., and Knowles, J. R. (1992) Segmental movement: Definition of the structural requirements for loop closure in catalysis by triosephosphate isomerase. *Biochemistry* 31, 8482–8487.

- (24) Sampson, N. S., and Knowles, J. R. (1992) Segmental motion in catalysis: Investigation of a hydrogen bond critical for loop closure in the reaction of triosephosphate isomerase. *Biochemistry* 31, 8488–8494.

- (25) Xiang, J., Jung, J.-y., and Sampson, N. S. (2004) Entropy effects on protein hinges: The reaction catalyzed by triosephosphate isomerase. *Biochemistry* 43, 11436–11445.

- (26) Xiang, J., Sun, J., and Sampson, N. S. (2001) The importance of hinge sequence for loop function and catalytic activity in the reaction catalyzed by triosephosphate isomerase. *J. Mol. Biol.* 307, 1103–1112.

- (27) Malabanan, M. M., Amyes, T. L., and Richard, J. P. (2010) A role for flexible loops in enzyme catalysis. *Curr. Opin. Struct. Biol.* 20, 702–710.

- (28) Wang, Y., Berlow, R. B., and Loria, J. P. (2009) Role of Loop-Loop Interactions in Coordinating Motions and Enzymatic Function in Triosephosphate Isomerase. *Biochemistry* 48, 4548–4556.

- (29) Kursula, I., Salin, M., Sun, J., Norledge, B. V., Haapalainen, A. M., Sampson, N. S., and Wierenga, R. K. (2004) Understanding protein lids: Structural analysis of active hinge mutants in triosephosphate isomerase. *Protein Eng., Des. Sel.* 17, 375–382.

- (30) Amyes, T. L., and Richard, J. P. (2007) Enzymatic Catalysis of Proton Transfer at Carbon: Activation of Triosephosphate Isomerase by Phosphite Dianion. *Biochemistry* 46, 5841–5854.

- (31) Amyes, T. L., Richard, J. P., and Tait, J. J. (2005) Activation of orotidine 5'-monophosphate decarboxylase by phosphite dianion: The whole substrate is the sum of two parts. *J. Am. Chem. Soc.* 127, 15708–15709.

- (32) Goryanova, B., Amyes, T. L., Gerlt, J. A., and Richard, J. P. (2011) OMP Decarboxylase: Phosphodianion Binding Energy Is Used To Stabilize a Vinyl Carbanion Intermediate. *J. Am. Chem. Soc.* 133, 6545–6548.
- (33) Amyes, T. L., Wood, B. M., Chan, K., Gerlt, J. A., and Richard, J. P. (2008) Formation and Stability of a Vinyl Carbanion at the Active Site of Orotidine 5'-Monophosphate Decarboxylase: pK_a of the C-6 Proton of Enzyme-Bound UMP. *J. Am. Chem. Soc.* 130, 1574–1575.
- (34) Tsang, W.-Y., Amyes, T. L., and Richard, J. P. (2008) A Substrate in Pieces: Allosteric Activation of Glycerol 3-Phosphate Dehydrogenase (NAD⁺) by Phosphite Dianion. *Biochemistry* 47, 4575–4582.
- (35) Ray, W. J., Jr., Long, J. W., and Owens, J. D. (1976) An analysis of the substrate-induced rate effect in the phosphoglucomutase system. *Biochemistry* 15, 4006–4017.
- (36) Kholodar, S. A., and Murkin, A. S. (2013) DXP Reductoisomerase: Reaction of the Substrate in Pieces Reveals a Catalytic Role for the Nonreacting Phosphodianion Group. *Biochemistry* 52, 2302–2308.
- (37) Amyes, T. L., and Richard, J. P. (2013) Specificity in Transition State Binding: The Pauling Model Revisited. *Biochemistry* 52, 2021–2035.
- (38) Jencks, W. P. (1975) Binding Energy, Specificity and Enzymic Catalysis: The Circe Effect. *Adv. Enzymol. Relat. Areas Mol. Biol.* 43, 219–410.
- (39) Wang, C., Rance, M., and Palmer, A. G. (2003) Mapping Chemical Exchange in Proteins with MW > 50 kD. *J. Am. Chem. Soc.* 125, 8968–8969.
- (40) Igumenova, T. I., and Palmer, A. G. (2006) Off-Resonance TROSY-Selected R1 ρ Experiment with Improved Sensitivity for Medium- and High-Molecular-Weight Proteins. *J. Am. Chem. Soc.* 128, 8110–8111.
- (41) Casteleijn, M. G., Alahuhta, M., Groebel, K., El-Sayed, I., Augustyns, K., Lambear, A.-M., Neubauer, P., and Wierenga, R. K. (2006) Functional role of the conserved active site proline of triosephosphate isomerase. *Biochemistry* 45, 15483–15494.
- (42) O'Connor, E. J., Tomita, Y., and McDermott, A. E. (1994) Synthesis of (1,2-C-¹³C₂) 2-Phosphoglycolic acid. *J. Labelled Compd. Radiopharm.* 34, 735–740.
- (43) Desai, K. K., and Miller, B. G. (2008) A Metabolic Bypass of the Triosephosphate Isomerase Reaction. *Biochemistry* 47, 7983–7985.
- (44) Sun, J., and Sampson, N. S. (1999) Understanding Protein Lids: Kinetic Analysis of Active Hinge Mutants in Triosephosphate Isomerase. *Biochemistry* 38, 11474–11481.
- (45) Gasteiger, E., Hoogland, C., Gattiker, A., Duvaud, S., Wilkins, M. R., Appel, R. D., and Bairoch, A. (2005) Protein identification and analysis tools on the ExPASy server. *Proteomics Protoc. Handb.*, 571–607.
- (46) Gasteiger, E., Gattiker, A., Hoogland, C., Ivanyi, I., Appel, R. D., and Bairoch, A. (2003) ExPASy: The proteomics server for in-depth protein knowledge and analysis. *Nucleic Acids Res.* 31, 3784–3788.
- (47) Borchert, T. V., Pratt, K., Zeelen, J. P., Callens, M., Noble, M. E. M., Opperdoes, F. R., Michels, P. A. M., and Wierenga, R. K. (1993) Overexpression of trypanosomal triosephosphate isomerase in *Escherichia coli* and characterization of a dimer-interface mutant. *Eur. J. Biochem.* 211, 703–710.
- (48) Glasoe, P. K., and Long, F. A. (1960) Use of glass electrodes to measure acidities in deuterium oxide. *J. Phys. Chem.* 64, 188–190.
- (49) Go, M. K., Amyes, T. L., and Richard, J. P. (2009) Hydron Transfer Catalyzed by Triosephosphate Isomerase. Products of the Direct and Phosphite-Activated Isomerization of [1-¹³C]-Glycolaldehyde in D₂O. *Biochemistry* 48, 5769–5778.
- (50) Plaut, B., and Knowles, J. R. (1972) pH-Dependence of the triosephosphate isomerase reaction. *Biochem. J.* 129, 311–320.
- (51) Amyes, T. L., and Richard, J. P. (1996) Determination of the pK_a of Ethyl Acetate: Bronsted Correlation for Deprotonation of a Simple Oxygen Ester in Aqueous Solution. *J. Am. Chem. Soc.* 118, 3129–3141.
- (52) Amyes, T. L., and Richard, J. P. (1992) Generation and stability of a simple thiol ester enolate in aqueous solution. *J. Am. Chem. Soc.* 114, 10297–10302.
- (53) Go, M. K., Malabanan, M. M., Amyes, T. L., and Richard, J. P. (2010) Bovine Serum Albumin-Catalyzed Deprotonation of [1-¹³C]-Glycolaldehyde: Protein Reactivity toward Deprotonation of α -Hydroxy α -Carbonyl Carbon. *Biochemistry* 49, 7704–7708.
- (54) Malabanan, M. M., Go, M. K., Amyes, T. L., and Richard, J. P. (2011) Wildtype and engineered monomeric triosephosphate isomerase from *Trypanosoma brucei*: Partitioning of reaction intermediates in D₂O and activation by phosphite dianion. *Biochemistry* 50, 5767–5779.
- (55) Misset, O., Bos, O. J., and Opperdoes, F. R. (1986) Glycolytic enzymes of *Trypanosoma brucei*. Simultaneous purification, intraglycosomal concentrations and physical properties. *Eur. J. Biochem.* 157, 441–453.
- (56) Wierenga, R. K., Noble, M. E. M., and Davenport, R. C. (1992) Comparison of the refined crystal structures of liganded and unliganded chicken, yeast and trypanosomal triosephosphate isomerase. *J. Mol. Biol.* 224, 1115–1126.
- (57) Alahuhta, M., and Wierenga, R. K. (2010) Atomic resolution crystallography of a complex of triosephosphate isomerase with a reaction-intermediate analog: New insight in the proton transfer reaction mechanism. *Proteins: Struct., Funct., Bioinf.* 78, 1878–1888.
- (58) Zhang, Z., Sugio, S., Komives, E. A., Liu, K. D., Knowles, J. R., Petsko, G. A., and Ringe, D. (1994) Crystal Structure of Recombinant Chicken Triosephosphate Isomerase-Phosphoglycolohydroxamate Complex at 1.8-Å Resolution. *Biochemistry* 33, 2830–2837.
- (59) Wierenga, R. K., Kapetanidou, E. G., and Venkatesan, R. (2010) Triosephosphate isomerase: A highly evolved biocatalyst. *Cell. Mol. Life Sci.* 67, 3961–3982.
- (60) Putman, S. J., Coulson, A. F. W., Farley, I. R. T., Riddleston, B., and Knowles, J. R. (1972) Specificity and kinetics of triosephosphate isomerase from chicken muscle. *Biochem. J.* 129, 301–310.
- (61) Hartman, F. C., LaMuraglia, G. M., Tomozawa, Y., and Wolfenden, R. (1975) The influence of pH on the interaction of inhibitors with triosephosphate isomerase and determination of the pK_a of the active-site carboxyl group. *Biochemistry* 14, 5274–5279.
- (62) Wolfenden, R. (1972) Analog approaches to the structure of the transition state in enzyme reactions. *Acc. Chem. Res.* 5, 10–18.
- (63) Wolfenden, R. (1969) Transition state analogues for enzyme catalysis. *Nature* 223, 704–705.
- (64) Goryanova, B., Spong, K., Amyes, T. L., and Richard, J. P. (2013) Catalysis by Orotidine 5'-Monophosphate Decarboxylase: Effect of 5-Fluoro and 4'-Substituents on the Decarboxylation of Two-Part Substrates. *Biochemistry* 52, 537–546.
- (65) Amyes, T. L., Ming, S. A., Goldman, L. M., Wood, B. M., Desai, B. J., Gerlt, J. A., and Richard, J. P. (2012) Orotidine 5'-monophosphate decarboxylase: Transition state stabilization from remote protein-phosphodianion interactions. *Biochemistry* 51, 4630–4632.
- (66) Barnett, S. A., Amyes, T. L., Wood, B. M., Gerlt, J. A., and Richard, J. P. (2008) Dissecting the Total Transition State Stabilization Provided by Amino Acid Side Chains at Orotidine 5'-Monophosphate Decarboxylase: A Two-Part Substrate Approach. *Biochemistry* 47, 7785–7787.
- (67) Barnett, S. A., Amyes, T. L., McKay, W. B., Gerlt, J. A., and Richard, J. P. (2010) Activation of R235A Mutant Orotidine 5'-Monophosphate Decarboxylase by the Guanidinium Cation: Effective Molarity of the Cationic Side Chain of Arg-235. *Biochemistry* 49, 824–826.
- (68) Jencks, W. P. (1981) On the attribution and additivity of binding energies. *Proc. Natl. Acad. Sci. U.S.A.* 78, 4046–4050.
- (69) Noble, M. E., Zeelen, J. P., and Wierenga, R. K. (1993) Structures of the "open" and "closed" state of trypanosomal triosephosphate isomerase, as observed in a new crystal form: Implications for the reaction mechanism. *Proteins* 16, 311–326.
- (70) Kursula, I., and Wierenga, R. K. (2003) Crystal structure of triosephosphate isomerase complexed with 2-phosphoglycolate at 0.83 Å resolution. *J. Biol. Chem.* 278, 9544–9551.

(71) Jogl, G., Rozovsky, S., McDermott, A. E., and Tong, L. (2003) Optimal alignment for enzymatic proton transfer: Structure of the Michaelis complex of triosephosphate isomerase at 1.2-Å resolution. *Proc. Natl. Acad. Sci. U.S.A.* 100, 50–55.

(72) Donnini, S., Groenhof, G., Wierenga, R. K., and Juffer, A. H. (2006) The planar conformation of a strained proline ring: A QM/MM study. *Proteins* 64, 700–710.